Electromigration in transition metals. III. Substitutional impurities in Cu, Ag, Al and Nb

1991 J. Phys.: Condens. Matter 3 8403

(http://iopscience.iop.org/0953-8984/3/43/007)

J. Phys.: Condens. Matter 3 (1991) 8403–8416. Printed in the UK

Electromigration in transition metals: III. Substitutional impurities in Cu, Ag, Al and Nb

J van Ek and A Lodder

Faculteit der Natuurkunde en Sterrenkunde, Vrije Universiteit, De Boelelaan 1081, 1081 HV Amsterdam, The Netherlands

Received 22 February 1991, in final form 5 August 1991

Abstract. Using the KKR Green function method, the electromigration wind valences of several substitutional impurities in Al and in the transition metals Cu, Ag and Nb have been calculated. In a complete migration jump the migrating ion exchanges position with a neighbouring vacancy. The present study is limited to the initial position in such a migration jump and to points along the migration path near to it. The complete band structure as well as all multiple scattering effects for the impurity cluster embedded in a crystal have been accounted for. For self-electromigration in Cu, Ag and Nb a positive wind valence is calculated while in Al the wind valence is negative. Sb in Ag has a large negative wind valence at the initial position. The constructed potentials for Cr and Fe in Nb yield negative wind valences for the impurities. It is concluded that the saddle-point configuration, where the impurity is midway along the path, generally will provide a large contribution to the average wind valence along the path.

1. Introduction

In a metal sample an electric field $\boldsymbol{E}$ and the accompanying current give rise to a cathode- or anode-directed flow of atoms. At moderate temperatures interstitial hydrogen is known to jump, at an appreciable rate, from one interstitial site to a neighbouring one. Larger atoms, located at lattice sites, are generally assumed to derive their mobility from repeated position exchange with neighbouring vacancies. An abundant vacancy fraction in the metal thus ensures an appreciable diffusion coefficient. Although in any sample vacancies are present a sufficiently high concentration is only reached at higher temperatures. Electromigration experiments are therefore commonly done at temperatures way above room temperature. In pure metal samples the direction of the self-diffusion by an electric field leads to self-electromigration. The electric field in an electromigration experiment on binary alloys induces two correlated atomic currents J_{host} and J_{impurity} of the host metal and substitutional impurity atoms respectively. This correlation is due to two species competing to exchange positions with a vacancy which is a common neighbour to host metal atoms as well as to the impurity.

In the phenomenologic description of electromigration in binary alloys the different atomic currents are given in terms of the apparent effective valences Z_α^{**} of the species under consideration

$$J_\alpha = L_{\alpha\alpha} Z_\alpha^{**} e\boldsymbol{E}. \tag{1}$$

0953-8984/91/438403+14$03.50

Here α stands for the host metal or the impurity, $L_{\alpha\alpha}$ is a diagonal Onsager transport coefficient and $e \equiv |e|$ is the elementary charge. The driving force in electromigration can be written as

$$F_\alpha = Z^*_\alpha e E. \tag{2}$$

The effective valence Z^*_α and apparent effective valence Z^{**}_α are related through [1, 2]

$$Z^{**}_\alpha = Z^*_\alpha + \frac{L_{\alpha\beta}}{L_{\alpha\alpha}} Z^*_\beta \qquad (\alpha \neq \beta). \tag{3}$$

The ratio $L_{\alpha\beta}/L_{\alpha\alpha}$ is found to lie in the range -2 to $+2$ depending on the alloy composition (see, for instance, [3] and [4]). Apparent effective valences have been determined experimentally for numerous alloys. On the basis of available information on jump frequencies, which serve as parameters in the kinetic model of impurity diffusion (for a review see [1] and [4]), Ho and Kwok [4] were able to extract the previously mentioned ratio of transport coefficients and in this way obtained Z^*_{impurity} values in Cu, Ag and Al based alloys.

Theoretical investigations on the effective valence in electromigration often utilize a distinction between the so-called direct valence of the species α, $Z_{\alpha,\text{direct}}$ and the wind valence $Z_{\alpha,\text{wind}}$. The direct valence describes the direct action of the electric field on the α-atoms. The response to the field-induced non-equilibrium distribution of the electrons in the metal is given by Z_{wind}. In many cases [1] the wind valence is large and negative and dominates a possible direct valence contribution. Such a negative wind valence indicates that the atom (of species α or β) is driven in the direction of the electron flow as if an electron wind pushes against the atom. In [5] it was shown that the wind valence of hydrogen in transition metals can be calculated successfully. These stimulating results invite further research into the class of substitutional impurities in metals.

Amongst earlier computational efforts there are the finite cluster calculations for model (spherical well) potentials by Sorbello *et al* [6] and finite cluster calculations on Nb based alloys by Brand and Lodder [7]. In a series of two articles [3, 8] Gupta *et al* investigated the wind valence for impurities in the noble metals and in Nb. Pseudo (model) potential calculations on Al based alloys have been reported by Sorbello [9, 10]. In spite of their pioneering character neither of the previously mentioned studies used methods which had typical solid state features or could be applied to transition metals.

A complete description of electron–impurity scattering in any metal, however, is available [11] within the KKR Green function formalism. All facets of the scattering of Bloch electrons by an impurity cluster embedded in an otherwise perfect crystal can be accounted for. The corresponding computational scheme, however, will be time consuming. It therefore seems sensible to perform a pilot study which focuses on the substitutional impurity at and just around its initial position in a migration jump towards a neighbouring vacancy. After minor changes the computer program used in the context of interstitial impurities [5, 12] perfectly suits this purpose.

Attention will be directed towards alloys based on Cu, Ag, Al and Nb as host metals. In section 2 relevant formulae that occur in calculating the electromigration wind valence are presented concisely. The muffin tin (MT) potentials that enter the calculation will be described. Paths along which electromigration of substitutional impurities in FCC and BCC metals is thought to proceed are given.

The results of wind valence calculations at or just around the initial position of the migrating impurity are presented in sections 4 and 5. The influence of the presence of the vacancy is investigated by comparing the wind valence $Z_{\alpha,\mathrm{wind}}$ of an impurity next to a vacancy with the wind valence of the same impurity, but now lacking a neighbouring vacancy. The influence of environmental effects as well as the dependence of $Z_{\alpha,\mathrm{wind}}$ on the fulfilment of the Friedel sum rule is discussed. In order to compare calculated results with experimental data, a calculation of $Z_{\alpha,\mathrm{wind}}$ should cover the entire migration path. Nevertheless the present results already show very interesting features, including a favourable comparison beforehand.

The final section summarizes the main points made in this study, and a forthcoming study is in prospect.

2. Calculation of the wind valence

The expression for the wind force on an atom, with its nucleus located at $\boldsymbol{R}_n$, is given by

$$F_{\mathrm{wind}}(\boldsymbol{R}_n) = \sum_k f(\epsilon_k) \left\langle \overline{\Psi}_k(\boldsymbol{r};\boldsymbol{R}_n) \right| - \nabla_{\boldsymbol{R}_n} v_n(\boldsymbol{r}-\boldsymbol{R}_n) \left| \overline{\Psi}_k(\boldsymbol{r};\boldsymbol{R}_n) \right\rangle . \quad (4)$$

The non-equilibrium part of the distribution function $f(\epsilon_k)$ for the electrons in alloy eigenstates $\overline{\Psi}_k$, at energy ϵ_k, is taken to be linear in the external field. The band index and the wavevector $\boldsymbol{k}$ have been combined in the single label k. The electron–impurity interaction for the migrating atom, at $\boldsymbol{R}_n$, is given by v_n. Expression (4), originally derived for an impurity in a jellium [13] could be successfully adapted to the band structure of real metals. In the present study equation (4) will be applied to substitutional impurities in metals. Note that v_n does not stand for the potential difference between the original host atom and the impurity atom. This potential difference, however, is responsible for the scattering of Bloch electrons and is accounted for through the alloy wavefunction $\overline{\Psi}_k$. The resulting electron density $|\overline{\Psi}_k|^2$ in the eigenstate labelled with k, interacts with the moving entity through v_n. The negative gradient of this interaction, summed over all scattering states weighted by the non-equilibrium electron distribution, gives rise to the wind force

$$F_{\mathrm{wind}}(\boldsymbol{R}_n) = Z_{\mathrm{wind}}(\boldsymbol{R}_n) e\boldsymbol{E}. \quad (5)$$

where $Z_{\mathrm{wind}}(\boldsymbol{R}_n)$ is the position-dependent 3×3 wind valence tensor which, when elaborated in the KKR Green function formalism, takes the form

$$Z_{\mathrm{wind}}(\boldsymbol{R}_n) = 2\epsilon_F \sum_L \sum_{m_1=-(l+1)}^{l+1} \left[\cot \eta^n_{l+1} - \cot \eta^n_l\right] D_{Ll+1,m_1} \mathrm{Re}\left[t^{n*}_{l+1} t^n_l W^n_{l+1,m_1,L}\right] . \quad (6)$$

The phase shifts η^n_l and the t-matrices t^n_l pertain to the MT potential for the atom at $\boldsymbol{R}_n$. L stands for the combination (l,m). Angular momenta up to $l_{\max} = 3$ are taken into account. The vectorial matrix

$$\boldsymbol{W}^n_{LL'} = \int_{FS} \frac{\mathrm{d}S_k}{v_k} \overline{C}^*_{nL}(k) \boldsymbol{\lambda}_k \overline{C}_{nL'}(k) \quad (7)$$

is an integral over the Fermi surface (FS). In equation (7) the integrand consists of the product of alloy wavefunction coefficients $C_{nL}(k)$ for the atom at R_n and the vector mean free path λ_k. In the isotropic relaxation time approximation the latter reads as τv_k, a product of the transport relaxation time τ and the group velocity v_k for an electron in the Bloch state $|k\rangle$. $W^n_{LL'}$ forms a dyadic product with $D_{LL'}$, the latter being proportional to a Gaunt coefficient. Apart from $D_{LL'}$ all quantities in equations (6) and (7) are energy-dependent but are to be evaluated at the Fermi energy ϵ_F. For more detailed information the reader is referred to [12].

The wind valence as presented in equation (6) allows for the determination of $Z_{\text{wind}}(R_n)$ of the impurity but also of the perturbed surrounding atoms in the cluster. A severe limitation, however, is formed by the fact that at present the alloy wavefunction coefficients can only be evaluated at lattice sites or slightly removed from them via a series expansion [14] of the wavefunction. That is why the present study is restricted to positions of the migrating atom at or just around the lattice site. Figures 1 and 2 show units cells in FCC and BCC lattices respectively. In both cells the central atom is missing and all atoms in the first shell in principle can exchange position with the vacancy. In pure samples this leads to self-diffusion. In dilute alloys one of the first shell atoms can be an impurity atom in competition with the other first shell atoms to exchange position with the vacancy. The wind valence of the host metal atom next to a vacancy in the pure sample can be different from that in the alloy. Note that in a perfect crystal the tensor $Z_{\text{wind}}(R_j)$, with R_j pointing towards a lattice site, although being identically zero does not vanish trivially, for η^j_l, t^j_l and $W^j_{LL'}$ all have non-zero elements.

Half the lengths of the migration paths depicted in figures 1 and 2 are $\frac{1}{4}\sqrt{2}a$ and $\frac{1}{4}\sqrt{3}a$ for FCC and BCC systems respectively, where a is the lattice constant. The previously mentioned series expansion of the wavefunction will be carried out to at most $0.03a$ along the path. Although this is only about one-tenth of the distance towards the so-called saddle-point configuration midway along the jump, trends in the variation of $Z_{\text{wind}}(R_n)$ along the path should show up. Nevertheless one must bear in mind that a huge contribution to the wind valence is to be expected from the impurity located at the saddle-point forming the 'activated complex' [1].

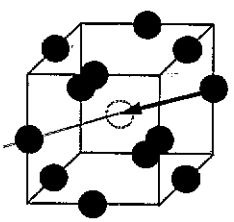

Figure 1. An FCC unit cell with a vacancy at its centre. The migrating atom is black but can either be a host atom or an impurity atom. It can move towards the vacancy along the [110] direction.

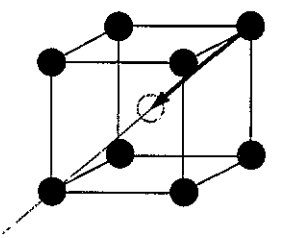

Figure 2. A BCC unit cell with a vacancy at its centre. The migrating atom can move towards the vacancy along the [111] direction.

In order to reduce the 3 × 3 wind valence tensor to a scalar quantity the same reasoning is followed as for the interstitial impurities [5]. What is measured in an

electromigration experiment is the effect of the component of the driving force in the direction in which the atom under consideration is mobile, i.e. along the migration path. In polycrystalline samples, for the wind part of the driving force, this leads to

$$F_{\text{wind}} = \left[\int_0^l \mathrm{d}s\, \hat{s} \cdot \boldsymbol{Z}_{\text{wind}}(s)\hat{s}P(s)\right] eE \equiv Z_{\text{wind}} eE. \tag{8}$$

$P(s)$ is the probability density of finding the atom at position $s \equiv s(\boldsymbol{R}_n)$ along the path of length l. The tangent unit vectors are defined through $\hat{s} \equiv \hat{s}(s)$. Here only values of

$$Z_{\text{wind}}(s) \equiv \hat{s} \cdot \boldsymbol{Z}_{\text{wind}}(s)\hat{s} \tag{9}$$

for small values of s will be calculated. For FCC systems one sees from figure 1 that $\hat{s} = (1/\sqrt{2}, 1/\sqrt{2}, 0)^t$ while in the BCC system in figure 2 $\hat{s} = (1/\sqrt{3}, 1/\sqrt{3}, 1/\sqrt{3})^t$.

The impurity phase shifts that enter the calculation via equations (6) and (7) have been derived from spherically symmetric MT potentials. These potentials are constructed from relativistic atomic charge densities [15] and have already proved their value in the context of interstitial electromigration [5] and the calculation of de Haas–van Alphen scattering quantities in $Pd(H)$[16]. Possible deviations from charge neutrality are monitored through a generalized Friedel sum rule [16, 17] and can be nullified via an approved shift procedure [16, 18–20]. This cannot be done in a meaningful way for all configurations. One of the reasons is that the clusters shown in figures 1 and 2 do not always form the complete environment of the defect. This point will be re-addressed in section 4.

The description of the different host metals addressed in this work is the same as has been used in the calculation of the wind valence of the light interstitials [5] and for the residual resistivity of impurities in transition metals [21]. This means that for FCC metals the MT radius was taken at $0.325a$ (touching spheres: $\frac{1}{4}\sqrt{2}a$). For BCC metals a relatively smaller MT radius of $0.335a$ (touching spheres: $\frac{1}{4}\sqrt{3}a$) was used which, however, gave quite satisfactory results for the residual resistivity of hydrogen in V, Nb and Ta [21].

The potentials for the substitutional impurities in Cu, Ag and Al selected for consideration in this work have in common that the residual resistivity they cause could be reproduced at least qualitatively (Sb in Ag) but often to a better extent (a vacancy or Ag in Cu or Cu in Al). For the Nb alloys, impurities such as Ta, Cr and Fe, which have been considered in previous studies [3, 7], have been selected. For these impurities only the residual resistivity of Nb(Ta) is known [22].

3. Experimental data and transport relaxation time

Table 1 shows effective valences as derived from experimental apparent effective valences by means of equation (3). For self-electromigration Z_α^{**} and Z_α^* are related simply by

$$Z_\alpha^{**} = Z_\alpha^*/f \tag{10}$$

where the correlation factor f equals 0.781 for jumps via a vacancy mechanism in FCC metals and $f = 0.727$ for the equivalent mechanism in BCC metals [1].

Table 1. Effective valences Z^* derived from apparent effective valences Z^{**} for various metals and dilute alloys. The average transport relaxation time τ was calculated from the bulk resistivity at temperature T.

System	Z^*	Z^{**}	T/K	τ/au	Reference
Cu in Cu	−4.1	−5.2	1200	130	[2]
Ag in Cu	−20.7	−17			[1]
Ag in Ag	−6.5	−8.3	1100	160	[2]
Sb in Ag	−115	−90			[4]
Al in Al	−16.4	−21	800	42	[2]
Cu in Al	−6.8				[4]
Nb in Nb	4.0	5.5	2250	12	[3]
Ta in Nb	4.5 to 18.5	10.5			[3]
Cr in Nb	−9.0 to 5.0	−3.0			[3]
Fe in Nb	−9.9 to 4.1	−3.9			[3]

In FCC metal based dilute alloys Ho and Kwok [4] found that the ratio of the transport coefficients in equation (3) is always negative and varies between −1.4 (Au(Sn)) and −0.4 (Al(Cu)). For Ag in Cu an intermediate value of $L_{\alpha\beta}/L_{\alpha\alpha} = -0.9$ was used in table 1. For BCC alloys Gupta *et al* [3] stated that $L_{\alpha\beta}/L_{\alpha\alpha}$ might vary from −2.0 to +1.5 which gives rise to a wide range of Z^* values, as indicated in table 1.

The isotropic transport relaxation time τ in table 1 has been obtained from the bulk resistivity at the indicated temperature, at which the electromigration experiments took place. This procedure involves an integral of the group velocity over the constant energy surface at $\epsilon = \epsilon_F$ and has been described earlier by Gupta *et al* [3] and in [5]. For completeness it is mentioned that this Fermi surface integral was evaluated using a touching MT sphere representation of the host crystal potential, which is believed to give the most reliable electron group velocities.

4. Results for Cu, Ag and Al based alloys

In this section numerical results on the wind valence of substitutional atoms at or close to their starting position in a migration jump will be presented. An FCC impurity cluster contains up to 13 MT potentials (figure 1). If there is a vacancy among the MT potentials it was always chosen at the centre of the cluster. The migrating atom was chosen to be the one in the [110] direction. In fact it should make no difference which site in the first shell surrounding the vacancy was chosen to hold the migrating atom as long as the migration direction $\hat{s}$ in equation (9) is transformed accordingly. This has been verified in a test calculation.

Tables 2, 3 and 4 show data on Cu, Ag and Al based alloys respectively. The second column in these tables gives the number of perturbed sites N accounted for in the calculation. Whenever N equals 13 the complete cluster, as shown in figure 1, was taken into account whereas $N = 2$ means that only the complex of the vacancy and one perturbed atom have been embedded in an otherwise perfect crystal. The $N = 1$ case corresponds to a single site calculation in which the vacancy has been replaced by a host atom and therefore the impurity is unable to move. The third column gives the outcome of the generalized Friedel sum which in principle should equal the valence charge difference ΔZ induced by the impurity cluster. Fulfilment

of this sum rule can be attained by adding or subtracting a constant potential to all the MT potentials in the cluster and thus guarantees that ΔZ is accommodated in scattering states $\overline{\Psi}_k$. The last column shows the applied constant energy shifts in Rydberg atomic units. These shifts alter the scattering properties of the impurity cluster and are interpreted as a change in the amount of screening charge associated with the impurity cluster [16, 20]. Here it is stressed that the shift procedure was only applied in the self-electromigration and the immobilized impurity configurations. For other configurations with an impurity, the environment accounted for in the present calculation (figures 1 and 2) was not complete. The complete oblong defect cluster consists of 20 and 16 potentials in the FCC and BCC systems respectively. Columns 4 to 7 contain the calculated wind valences $Z_{\text{wind}}(s)$ along the path, starting from the stable position ($s = 0$) and entering the path towards the vacancy by a small amount (only up to $s = 0.03a$).

In Cu and Ag a vacancy, influencing the first shell, gives rise to a positive wind valence on the first shell atoms. This is remarkable, for the effective valence for self-electromigration is strongly negative in these metals. Apparently the saddle-point configuration must provide a huge negative contribution. When the potentials are made to fulfil the Friedel-sum rule, hence F-sum $= -1$ for a vacancy in Cu, the results are slightly altered. Note that for this value of -1 the contribution of -10 from the 10 d-electrons far below the Fermi level was omitted. The resistivity due to this shifted impurity cluster is known to be in good agreement with experiment [21]. Upon leaving the initial position, in the $N = 13$ cluster the Cu and Ag atoms experience a diminishing wind force in the direction of the field. This is to be expected because of the large negative effective valence in these metals. Apparently the $N = 2$ cluster is not capable of reproducing the expected behaviour since it leads to an initially increasing wind valence along the path in the [110] direction. Of course an initial increase of Z_{wind} followed by a decrease further on along the path cannot be excluded at this stage but would certainly constitute another unexpected feature. The last row in the host metal/vacancy sections of tables 2 and 3 carry '$A = 1$' as a comment. This indicates that all multiple (back) scattering effects in electron–impurity scattering, according to the KKR Green function description contained in the so-called A-matrix [23], have been neglected. This means that the alloy wavefunction coefficients $\overline{C}_{nL}(k)$ in (7) are replaced by host wavefunction coefficients. One then expects just a small deviation from the value of zero for the pure host because the first shell atoms are only slightly perturbed and strong backscattering is absent. This indeed is the case as can be seen from tables 2 and 3. In addition it was verified that an unperturbed Cu atom next to a vacancy experiences no wind force at all if $A = 1$.

For Ag in Cu a large negative wind valence, dominating possible direct valence contributions, can be deduced from the data in table 1. In table 2 the wind valence on Ag in a Cu matrix without and with an adjacent vacancy is given. If no vacancy is present, Ag has a small negative wind valence but the atom is unable to move from its site. This situation does not contribute to Z^{**}_{Ag} but causes a residual resistivity which is reproduced extremely well [21]. If a vacancy is present it greatly influences the wind valence. A change of sign and an increase by a factor of about ten in magnitude is seen from table 2. A calculation with $A = 1$ again leads to a negative wind valence in sharp contrast with a correct calculation resulting in $Z_{\text{wind}}(s) \approx 2$. Upon leaving the initial position $s = 0$ the $N = 13$ cluster as well as the $N = 2$ cluster show only minor variation in $Z_{\text{wind}}(s)$.

A huge wind valence is ascribed to Sb in Ag. The results in table 3 clearly reflect

Table 2. Wind valences $Z_{\text{wind}}(s)$ at ($s = 0$) and close to ($s = 0.01a, 0.02a, 0.03a$) the substitutional position of metal atoms in Cu. N is the number of MT spheres in the impurity cluster. The generalized Friedel-sum (F-sum) depends on the constant energy shift (in Ryd) given in the last column. The comment '$A = 1$' indicates that all backscattering effects have been neglected.

			$Z_{\text{wind}}(s)$				
System	N	F-sum	$s = 0$	$0.01a$	$0.02a$	$0.03a$	Comment
Cu(Cu,vac)	13	−0.61	1.14	—	—	—	0
	2	−0.25	1.05	—	—	—	0
	13	−1.03	1.25	1.20	1.09	0.96	0.012
	2	−0.30	1.04	1.15	1.23	1.30	0.012
	2	−0.31	−0.05	—	—	—	0, $A = 1$
Cu(Ag)	13	−0.46	−0.21	—	—	—	0
	1	−0.54	−0.16	—	—	—	0
	13	0.01	−0.38	—	—	—	−0.014
	1	−0.52	−0.07	—	—	—	−0.014
Cu(Ag,vac)	13	−1.06	2.14	2.18	2.18	2.16	0
	2	−0.79	2.09	2.13	2.16	2.15	0
	2	−0.94	−1.59	—	—	—	0, $A = 1$

Table 3. Wind valences $Z_{\text{wind}}(s)$ in Ag. See table 2 for further explanation.

			$Z_{\text{wind}}(s)$				
System	N	F-sum	$s = 0$	$0.01a$	$0.02a$	$0.03a$	Comment
Ag(Ag,vac)	13	−0.55	2.02	—	—	—	0
	2	−0.33	1.94	—	—	—	0
	13	−1.04	2.35	2.35	2.29	2.18	0.018
	2	−0.39	2.11	2.26	2.40	2.52	0.018
	2	−0.27	−0.04	—	—	—	0, $A = 1$
Ag(Sb)	13	2.72	−41.8	—	—	—	0
	1	2.61	−41.9	—	—	—	0
	13	4.03	−46.6	—	—	—	−0.050
	1	2.78	−47.8	—	—	—	−0.050
Ag(Sb,vac)	13	2.16	−46.1	−45.9	−45.8	−45.4	0
	2	2.37	−46.1	−45.9	−45.6	−45.3	0
	2	2.97	−57.3	—	—	—	0, $A = 1$

this experimental observation. Inclusion of all first shell atoms around the vacancy does not alter the wind valence significantly. Along the path only minor variations are detected pointing in the direction of a diminishing magnitude of the wind valence. This is at variance with the experimental value $Z^*_{\text{Sb}} = -115$ and probably will be overcome in more remote regions along the migration path. Note that the Friedel-sum rule criterion is by no means met in Ag (Sb, vac) (the F-sum should be $+4 - 1 = +3$). For the present purpose this is not very important although the wind valences are likely to be affected as can be seen from Ag (Sb).

An FCC metal that received much attention in the field of electromigration is Al. Electromigration-induced failure in Al conductor lines could be prevented by alloying Al with small amounts of Cu [4]. This means that Al and Al (Cu) are also interesting candidates for a closer investigation.

Table 4 indicates that an unshifted impurity cluster already fulfils the Friedel-sum rule to a large extent. Application of a small positive shift to the $N = 13$ cluster suffices to account completely for the three missing valence electrons. The perturbed Al atoms surrounding the vacancy feel a wind force proportional to the field by $Z_{\text{wind}}(0) \approx -2.4$. Upon leaving the lattice site the magnitude of the wind valence slowly increases. Again backscattering effects are very important as can be read from the last line in the Al (Al, vac) section of table 4.

Table 4. Wind valences $Z_{\text{wind}}(s)$ in Al. See table 2 for further explanation.

			$Z_{\text{wind}}(s)$				
System	N	F-sum	$s = 0$	$0.01a$	$0.02a$	$0.03a$	Comment
Al(Al,vac)	13	−2.84	−2.48	—	—	—	0
	2	−2.05	−2.38	—	—	—	0
	13	−3.01	−2.43	−2.45	−2.49	−2.52	0.004
	2	−2.07	−2.31	−2.39	−2.41	−2.43	0.004
	2	−2.36	0.37	—	—	—	0, $A = 1$
Al(Cu)	13	−2.70	−12.2	—	—	—	0
	1	−2.24	−12.4	—	—	—	0
	13	−2.02	−10.9	—	—	—	−0.014
	1	−2.13	−10.8	—	—	—	−0.014
Al(Cu,vac)	13	−5.48	−10.5	−10.5	−10.4	−10.3	0
	2	−4.28	−10.7	−10.6	−10.6	−10.5	0
	2	−4.44	−6.85	—	—	—	0, $A = 1$

An immobilized Cu atom has a wind valence of about −11. The addition of a vacancy next to the Cu atom does not alter the situation too much while the Friedel-sum shows that the 0.48 electron is missing.

Although the presence of the Cu atom probably influences the electromigration properties of the Al atoms in the cluster, the suppression of electromigration-induced failure of Al conductor lines is not likely to be the result of these local effects. As a matter of fact test calculations revealed only a minor influence of the Cu atom on the $Z_{\text{Al,wind}}(0)$. For the different non-equivalent Al atoms in the first shell surrounding the vacancy, effects ranging from a 7% decrease to a 4.5% increase in magnitude of the wind valence with respect to the Al(vac) system were found. Moreover, in a dilute Al(Cu) alloy, the majority of the Al atoms still migrate via a vacancy mechanism without being influenced at all by the scarce Cu atoms in the system. The reduction of the electromigration damage upon alloying Al with an amount of Cu exceeding the solubility limit (0.16%), is believed to be a grain boundary effect [4]. Excess Cu atoms inhibit the electromigration processes taking place on the boundaries of Al grains.

5. Results for Nb based alloys

Unlike Cu, Ag and Al, Nb is a true transition metal in the sense that a partially filled d-band at the Fermi level gives rise to a complicated electronic structure. Gupta *et al* [3] were the first to investigate the electromigration properties of several substitutional impurities in Nb by computational means. Although the electronic structure of the Nb host was accounted for, presumably important backscattering from the crystal

and the presence of the neighbouring vacancy had been neglected. The impurity wind valences Gupta *et al* ended up with were all very small, ranging from 0.043 for Cr to 0.094 for Ta.

Some years later Brand and Lodder [7] calculated the wind valence of Nb, Ta, Cr and Ni in Nb within a finite cluster model. Although a marked dependence on cluster size was seen, their results on the average were an order of magnitude larger than those of Gupta *et al* . Brand and Lodder did account for all multiple scattering effects within the cluster embedded in a free electron gas. This in fact explains the cluster size dependence they observed in their calculations. Because the Nb Fermi surface did not enter their calculation they extracted the transport relaxation time from the well-known free electron (FE) expression for the bulk resistivity and obtained $\tau_{FE} = 3.4$. If this value is compared with $\tau = 12$ in table 1, a difference of a factor of 3.5 emerges.

In the present work the complete Nb band structure as well as all multiple scattering effects in the system are accounted for. The results are shown in table 5 which is built up in the same way as tables 2–4. $N = 9$ corresponds to the full impurity cluster as shown in figure 2. A vacancy in an Nb lattice introduces a five-electron deficiency which can be accommodated in the impurity cluster by shifting the MT potentials rigidly over 0.034 Ryd. This shifting procedure reduces the wind valence from 1.33 to 0.48 in the $N = 9$ cluster. A slight displacement of the Nb atom in the direction of the vacancy results in a very rapid increase of the wind valence. Such a strong dependence of Bloch electron scattering on the position of the Nb atoms has also been encountered in the calculation of residual resistivities in Nb [21].

Clearly the scattering properties of the more complete $N = 9$ cluster cannot be described adequately by reducing it to just the vacancy and one perturbed Nb atom ($N = 2$). Note that already at $s = 0.03a$ the wind valence of Nb($Z_{wind}(0.03a) = 1.55$) exceeds the saddle-point value of Gupta *et al* by a factor of 8 and the value of Brand and Lodder ($Z_{wind} = 0.71$) by a factor of 2. If the results of Brand and Lodder are corrected for the previously mentioned difference in transport relaxation time, one finds a value of $Z_{wind} = 2.49$. This path-averaged value seems to be compatible with the data on the Nb(Nb,vac) system presented in table 5.

A test calculation on the Nb(Nb,vac) system using a larger host MT radius $R_{MT} = 0.391a$ shows that the unshifted potentials almost yield fulfilment of the Friedel-sum rule. The wind valence is influenced strongly by this increase in MT radius which is also reflected in residual resistivity calculations [21]. It will be interesting to use a self-consistent potential for this system which will become available in the near future [24].

Ta in Nb was seen to give a low residual resistivity when the [Xe] $4f^{14}5d^36s^2$ atomic ground state configuration was used in the construction of the impurity potentials. The alternative $5d^46s^1$ configuration resulted in larger residual resistivities which are in much better agreement with experiment. As for the wind valence, table 5 shows that the $5d^36s^2$ configuration gives rise to a substantial positive wind valence for both the immobilized Ta atom as well as the Ta atom next to a vacancy. The wind valence already increases significantly upon leaving the initial position by only a small distance. The $5d^46s^1$ Ta atomic configuration which yields the more reliable potential in view of the residual resistivity calculations, leads to smaller wind valences. After closer inspection this was found to be caused by a reversal of the sign of the $l = 1$ contribution in equation (6). Introduction of a vacancy next to a Ta $5d^46s^1$ atom reduces Z_{wind} to negative values but a tendency towards increasing (positive) values

Table 5. Wind valences $Z_{wind}(s)$ in Nb. See table 2 for further explanation.

System	N	F-sum	$Z_{wind}(s)$ $s=0$	$0.01a$	$0.02a$	$0.03a$	Comment
Nb(Nb,vac)	9	−2.71	1.33	1.07	0.67	0.08	0
	2	−1.68	1.18	0.99	0.69	0.23	0
	9	−5.08	0.48	0.88	1.22	1.55	0.034
	2	−2.00	−0.01	−0.11	−0.32	−0.69	0.034
	2	−2.34	−0.69	—	—	—	0, $A=1$
Nb(Nb,vac)	9	−4.87	1.39	1.15	0.94	0.74	0, $R_{MT}=0.391a$
Nb(Ta d^3s^2)	9	−0.54	2.99	—	—	—	0
	1	−0.39	2.94	—	—	—	0
	9	0.01	2.94	—	—	—	−0.008
	1	−0.33	2.93	—	—	—	−0.008
Nb(Ta d^3s^2,vac)	9	−3.20	2.64	3.16	3.62	4.04	0
	2	−2.07	2.40	2.95	3.46	3.92	0
	2	−2.62	−0.62	—	—	—	0, $A=1$
Nb(Ta d^4s^1)	9	−1.53	0.14	—	—	—	0
	1	−1.35	0.16	—	—	—	0
	9	0.05	0.82	—	—	—	−0.022
	1	−1.20	0.79	—	—	—	−0.022
Nb(Ta d^4s^1,vac)	9	−4.19	−1.08	−0.52	0.08	0.71	0
	2	−3.08	−1.26	−0.66	−0.04	0.63	0
	2	−3.46	−4.01	—	—	—	0, $A=1$
Nb(Cr)	9	0.95	−7.00	—	—	—	0
	1	1.24	−6.83	—	—	—	0
	9	1.09	−6.90	—	—	—	−0.002
	1	1.27	−6.80	—	—	—	−0.002
Nb(Cr,vac)	9	−1.68	−1.78	−1.66	−1.57	−1.51	0
	2	−0.54	−1.99	−1.84	−1.73	−1.63	0
	2	−1.33	−4.65	—	—	—	0, $A=1$
Nb(Fe)	9	−3.16	−1.58	—	—	—	0
	1	−2.61	−1.67	—	—	—	0
	9	3.09	−1.78	—	—	—	−0.058
	1	−2.41	−1.30	—	—	—	−0.058
Nb(Fe,vac)	9	−4.99	−0.10	0.06	0.21	0.33	0
	2	−3.71	−0.12	0.02	0.15	0.26	0
	2	−4.47	2.29	—	—	—	0, $A=1$

further on along the path, as observed in the Nb(Ta $5d^36s^2$) system, remains.

Contrary to previously published results [3, 7] a negative wind valence is calculated for Cr in Nb. The [Ar] $3d^54s^1$ atomic ground state configuration has been used in the potential construction. Upon the introduction of a vacancy the magnitude of the wind valence is significantly reduced. The variation of $Z_{wind}(s)$ of Cr in Nb as a function of s is moderate when compared with that of Ta in Nb.

For Fe (atomic configuration [Ar] $3d^64s^2$) also a negative wind valence is calculated, which is of smaller magnitude than that of Cr in Nb. Again the introduction of a vacancy next to the Fe atom quenches the magnitude of $Z_{wind}(0)$. On following the migration path again an increase is seen. A change of sign in $Z_{wind}(s)$ against s is observed. Note the remarkable influence of backscattering effects on $Z_{wind}(0)$ in the case of Nb(Fe,vac).

The experimental data on Nb alloyed with Cr and Fe, as given in table 1, offer room for a negative wind valence, even if one considers a possible direct valence contribution.

Theory [13, 25] tends to predict $Z_{\text{direct}} = Z_{\text{host}} = 5$ at the starting point and $Z_{\text{direct}} = 0$ at the saddle-point, which would result in an average of about +2.5 along the migration path. This value was also mentioned by Gupta *et al* [3]. In view of a recent analysis by Lodder [26] the actual value could be somewhat larger due to incomplete screening of the migrating ion. Incorporating this effect, it is seen from table 1 that even then the wind valence of Ta in Nb is bound to be positive.

Although the physical interpretation is not clear one can also calculate the wind valence of a vacancy in a metal. For a single vacancy in the FCC and BCC metals considered in this work a consistently negative wind valence is found, varying from −8.2 in Al to −2.8 in Cu. In order to see how these values arise the shape of a vacancy potential is depicted in figure 3(*a*). One notes a bump with a maximum value exceeding the Fermi energy thus providing a strongly repulsive potential. A negative wind valence for such a repulsive potential means that electrons at the Fermi energy, the majority incoming from the right-hand side in figure 3(*a*), are scattered into states that propagate towards the right-hand side. The resultant increase in electronic charge density on the right of the vacancy exerts an electrostatic force on the vacancy in the direction opposite to the field direction, i.e. $Z_{\text{vac.,wind}} < 0$. The precise distribution of the field-induced charge density around the vacancy determines the wind force on the neighbouring atoms. Evidently, in for instance Nb, this distribution is such that more negative charge is located on the right-hand side of the neighbouring metal atom, located at $\boldsymbol{R}_1$ in figure 3(*a*). In neglecting multiple scattering effects between the vacancy and the surrounding atoms, the interference between incoming and outgoing states is altered. Now negative charge is found between the vacancy and the atom to its right-hand side.

When the atom next to the vacancy starts to move in the direction of the vacancy (figures 3(*b*) and 3(*c*)), the height of the bump will diminish. As a consequence the vacancy potential will become less repulsive and the charge accumulated to the right of what remains of the vacancy will diminish. If the previously mentioned reasoning is correct, replacement of the vacancy MT potential by a constant potential at the MT zero of the host metal also should result in a reduction of $Z_{\text{wind}}(0)$ of the first shell atoms. Actual test calculations on Cu(vac) with $\eta_l^{\text{vac.}} = 0$ indeed show that the wind valence on Cu reduces from 1.14 (see table 2) to 0.99. For Ag the reduction is from 2.02 to 0.86. In addition these results indicate that the effect of the vacancy on the wind valence of the first shell atoms is modelled to some extent simply by a flat potential.

6. Conclusions and outlook

In this article first results on calculated wind valences for substitutional impurities in transition metals have been presented. At the present stage only the initial position of an impurity next to a vacancy is covered, which implies that a detailed comparison with experiment cannot yet be made. Both multiple scattering and band structure effects, which had been neglected in previous studies [3, 7] have now been accounted for exactly within the KKR Green function formalism.

It is found that the wind valence for the self-electromigration of Cu and Ag has a positive sign at and around the initial position. Z_{wind} decreases upon leaving the initial position towards the vacancy. Presumably this positive wind valence is a consequence of the redistribution of charge around the first shell atoms due to electron–vacancy

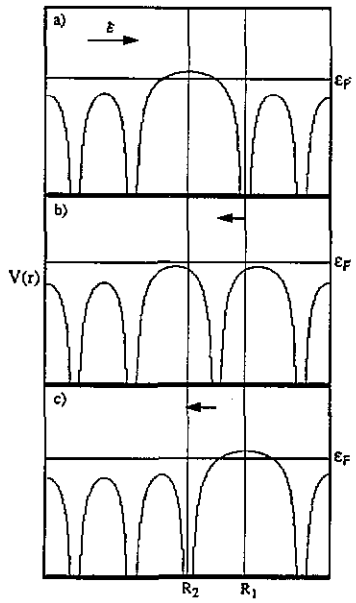

Figure 3. A one-dimensional schematic plot of the potential $V(r)$ at three points along the migration jump of an atom at R_1 towards a vacancy at R_2. (*a*) In the initial situation the vacancy shows up as a bump exceeding the Fermi level at energy ϵ_F. (*b*) Midway along the migrating atom causes the potential to lower. (*c*) The final situation is the mirror image of the initial situation. The migrating atom did exchange positions with the vacancy.

scattering, for the first shell atoms themselves are only weak scatterers when compared with host atoms.

A much stronger scatterer, such as Sb, next to a vacancy in Ag gives a huge negative wind valence which, in view of the experiment, should decrease even further upon approaching the saddle-point configuration in the migration jump. In the very small interval along the path, studied in this work, no trace of such a decrease has yet been found.

In Nb wind valences are found which are much larger than those published earlier. For Ta at its initial position in Nb a positive effective valence is to be expected on the basis of the calculated wind valence plus a possible direct valence contribution. For Cr and Fe a negative wind valence is calculated.

Neglect of backscattering effects was simulated by substitution of the identity matrix for the complex backscattering matrix (A-matrix). In most cases severe errors in the resulting wind valences were detected. In addition the representation of a missing atom next to the migrating atom by a true vacancy potential was shown to be important, at least in the initial configuration.

On the basis of the dependence of the presented wind valences on the cluster size it is concluded that in most cases the two-atom results do not show spectacular deviations from the $N = 13$ (FCC) or $N = 9$ (BCC) results, except for the self-electromigration in Nb. For the fulfilment of the Friedel-sum rule by means of a shifting procedure, the larger cluster has always been employed. This procedure applied to the $N = 2$ cluster would lead to the accumulation of an unrealistically large screening charge on the individual atoms.

For certain systems the results were found to be sensitive to the choice of the potential. In itself this is not surprising because only simply constructed potentials were used, starting from atomic charge densities corresponding to different electronic configurations. Also for the more complicated defects, characteristic for substitutional migration, a shift procedure for obtaining local charge neutrality becomes questionable. Apparently, in order to circumvent these problems, a self-consistent potential is becoming more and more indispensable.

The present results on the electromigration of substitutional impurities in transition metals are stimulating and indeed call for further inquiries. To this end an extended description [11], designed to treat clusters of an arbitrary shape embedded in an otherwise perfect crystal, must be implemented in full detail. After this has been realized the complete migration path can be accessed. The electron scattering at the saddle-point as well as the influence of lattice deformation and the temperature effects mentioned by Gupta *et al* [3] will then be investigated. Comparison of results at the initial position, to be obtained with the future computer program, should equal the results at $s = 0$ presented in this work. This provides a useful check for the validity of the future program.

As far as the direct valence is concerned, the average wind valence along the complete path will help to explain its nature by comparing it with experimental effective valences. In this respect impurities in host metals with a high number of valence electrons are interesting. At present a not-very-well-established value of $\frac{1}{2}Z_{\text{host}}$ is chosen. It should be possible to decide about the validity of this choice for hosts like Ni, Pd and Pt where $Z_{\text{host}} = 10$, containing impurities for which the wind valence does not dominate Z^* completely.

References

[1] Wever H 1973 *Elektro- und thermotransport in Metallen* (Leipzig: Barth)
[2] Huntington H B 1974 *Diffusion in Solids: Recent Developments* (New York: Academic) p 303
[3] Gupta R P, Serruys Y, Brebec G and Adda Y 1983 *Phys. Rev.* B **27** 672
[4] Ho P S and Kwok T 1989 *Rep. Prog. Phys.* **52** 301
[5] Ek J van and Lodder A 1991 *J. Phys.: Condens. Matter* **3** 7331
[6] Sorbello R S, Lodder A and Hoving S J 1982 *Phys. Rev.* B **25** 6178
[7] Brand M G E and Lodder A 1986 *Phys. Status Solidi* b **133** 119
[8] Gupta R P 1982 *Phys. Rev.* B **25** 5188
[9] Sorbell R S 1973 *J. Phys. Chem. Solids* **34** 937
[10] Sorbello R S 1981 *J. Phys. Chem. Solids* **42** 309
[11] Lodder A 1984 *J. Phys. F: Met. Phys.* **14** 2943
[12] van Ek J and Lodder A 1991 *J. Phys.: Condens. Matter* **3** 7307
[13] Bosvieux C and Friedel J 1962 *J. Phys. Chem. Solids* **23** 123
[14] Oppeneer P M and Lodder A 1988 *J. Phys. F: Met. Phys.* **18** 869
[15] Desclaux J P, Moser C M and Verhaegen G 1971 *J. Phys. B: At. Mol. Phys.* **4** 296
[16] Oppeneer P M and Lodder A 1987 *J. Phys. F: Met. Phys.* **17** 1901
[17] Lehmann G 1975 *Phys. Status Solidi* b **70** 737
[18] Mrosan E and Lehmann G 1976 *Phys. Status Solidi* b **78** 159
[19] Molenaar J, Coleridge P T and Lodder A 1981 *J. Phys. F: Met. Phys.* **11** 437
[20] Molenaar J, Lodder A and Coleridge P T 1983 *J. Phys. F: Met. Phys.* **13** 839
[21] van Ek J and Lodder A 1991 *J. Phys.: Condens. Matter* **3** 7363
[22] 1982 *Landolt-Börnstein New Series* vol 15a (Berlin: Springer)
[23] Lodder A 1976 *J. Phys. F: Met. Phys.* **6** 1885
[24] Zeller R 1991 private communication
[25] Lodder A 1989 *Physica* A **158** 723
[26] Lodder A 1991 *J. Phys.: Condens. Matter* **3** 399